Appendices to "A new convective instability of the rotating-disk boundary layer with growth normal to the disk"

By J. J. Healey *Journal of Fluid Mechanics*, vol. 560 (2006), pp. 279–310

Appendix A. Model problem with a pair of saddle-points

The integral definition of the Airy function,

$$\mathrm{Ai}(z) = \int_C \exp\left(zt - t^3/3\right)\ \mathrm{d}t, \tag{A 1}$$

where the integration path C goes from $\infty\exp(-2\pi\mathrm{i}/3)$ to $\infty\exp(2\pi\mathrm{i}/3)$, can be used to illustrate the behaviour of an integral with two saddle-points when $|z|$ is large. There are no singularities in the exponent, so the value of the integral does not depend on C, provided it has these end-points. This example is adapted from Hinch (1991), but here our focus is on the contribution, or otherwise, of the second saddle point. In fact $|z|$ need not be very large to use saddle-point theory to give good approximations to the right-hand side of (A 1), and we shall use $z = 3\mathrm{e}^{\mathrm{i}\theta}$ in what follows. The saddle points lie at $t = \pm\sqrt{z}$. Figure 1 shows how the saddles change height and move around the complex t-plane as θ is varied, and indicates integration paths that can pass over one or both saddles. The integration paths are chosen to remain within the valleys of the dominant saddles. When $\arg z = \pi$ both saddles are at the same height and make contributions of equal magnitude, otherwise the saddle in the left half-plane is dominant. The saddles also have equal height when $\arg z = \pi/3$, but in this case only the left-hand saddle makes a contribution.

Figure 2 shows the accuracy of theories that use both saddles, and only one saddle, near $\arg z = \pi/3$ and $\arg z = \pi$. Near $\arg z = \pi/3$ the theory based on the left-hand saddle alone is indistinguishable from the numerical solution, while near $\arg z = \pi$ the contribution from both saddle points is needed to obtain similar accuracy. Considering figures 1 and 2 together, it is apparent that it is necessary to study with particular attention the topology of the complex plane when near critical parameter values where two saddles are at the same height.

When $\arg z$ is reduced through $\pi/3$ the right-hand saddle becomes cut off from the integration path, but this does not produce a sharp change to the integral. As $\arg z$ approaches $\pi/3$ from above, the right-hand saddle's contribution to the integral reduces, even though its height is increasing. It can be seen from figure 1(e) that, as $\arg z \to \pi/3$ from above, a path remaining within the valley of the dominant saddle is constrained to lie closer and closer to the right-hand saddle, and first passes over this saddle from left to right before passing over it again from right to left. The contributions from these two passages near the right-hand saddle almost cancel, thereby reducing the contribution of the saddle, and leading to the smooth 'switch-off' of the saddle's contribution.

The situation where dominance changes from A to B between figures 5(a) and (b) of the main paper corresponds to the situation near $\arg z = \pi$ in figures 1(a), (b) and (c), and so both A and B contribute to the physical solution in figures 5(a) and (b) of the

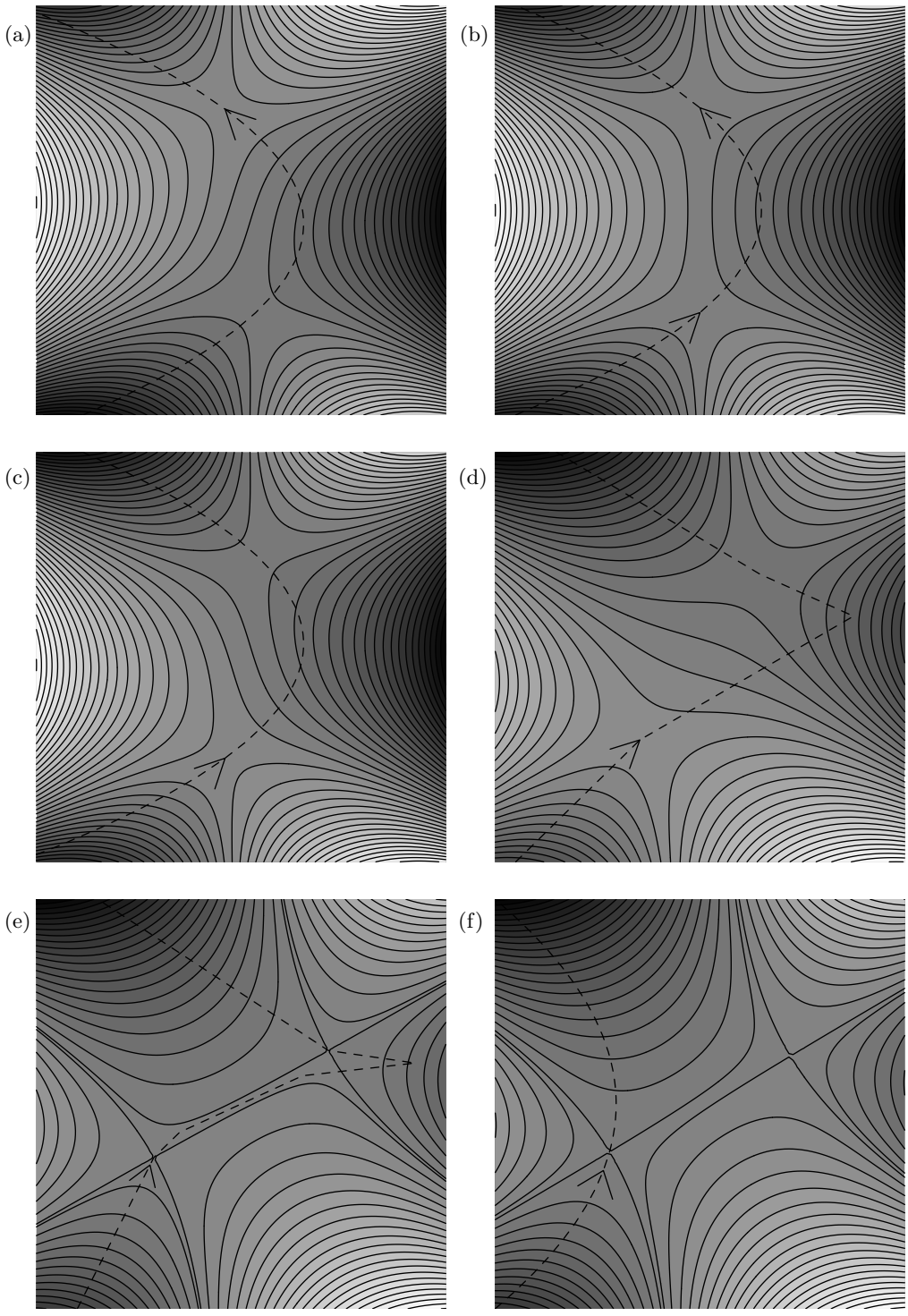

FIGURE 1. Complex t-planes showing contours of constant $\mathrm{Re}(zt - t^3/3)$ for (a) $\arg z = 1.1\pi$, (b) $\arg z = \pi$, (c) $\arg z = 0.9\pi$, (d) $\arg z = 0.6\pi$, (e) $\arg z = 0.35\pi$, (f) $\arg z = 0.31\pi$. Dashed lines indicate possible integration paths C, arrows show direction of integration and are placed near dominant saddles. Darker shading indicates more negative $\mathrm{Re}(zt - t^3/3)$.

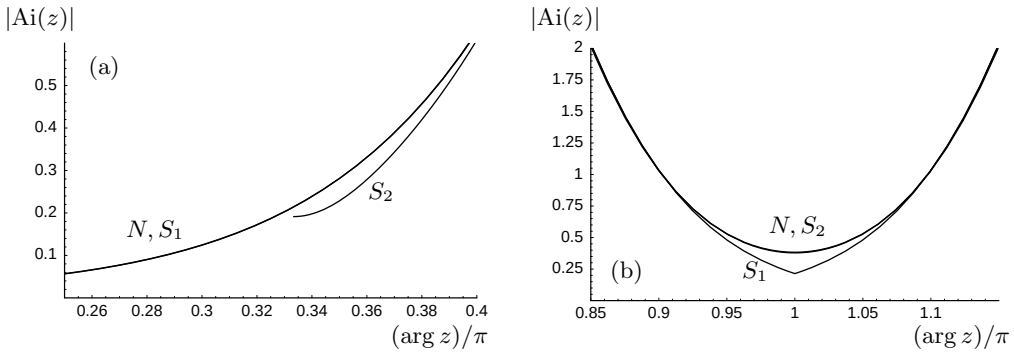

FIGURE 2. Comparison of saddle-point theories with numerical evaluation of the Airy function for $|z| = 3$. (a) Behaviour near $\arg z = \pi/3$; (b) behaviour near $\arg z = \pi$. In each diagram N refers to numerical evaluation of the Airy function, S_1 refers to the asymptotic theory based on the single dominant saddle and S_2 refers to the asymptotic theory based on using both saddle points.

main paper. The situation where A overtakes B in height between figures 5(b) and (c) of the main paper corresponds to the situation near $\arg z = \pi/3$ in figures 1(e) and (f), and so A is cut off, and only B contributes to the physical solution in figure 5(c) of the main paper.

Appendix B. Mapping out the complete unstable domain for an impulsive disturbance

The range of ρ/t is now extended beyond that shown in figures 9 and 10 of the main paper to include the rest of the unstable part of the impulse response. We start by considering the growth rates for $\zeta/t = 0$; these are shown in figure 3. The growth rate curves for saddles A, B and D have been extended, and five new unstable saddles, labelled E, F, G, H and I, have been found. Identifying the dominant saddle when there are so many saddles, and how the dominance changes when there are so many intersection points where saddles have coincident growth rates requires careful investigation of the branches in the complex α-plane. To illustrate the process, we show in figure 4 the complex α-plane at $\rho/t = 0.1342$, $\zeta/t = 0$, where figure 3 indicates that there are six saddles with comparable growth rates. These saddles are distributed over four Riemann surfaces, connected by three branch-points, from which branch-cuts have been drawn to allow the surfaces to be considered separately, like in figure 3 of the main paper. (There are really eight Riemann surfaces as each of the four has a corresponding surface of divergent eigenfunctions, but these have not been treated by separate diagrams).

At these parameter values, D, F, G, H and I are quasi-modes, and F is the dominant saddle. The quasi-modes G, H and I, although solutions of the inviscid initial-value problem, have an arrangement of critical points and branch-cuts that mean they are not likely to have any analogue in the corresponding viscous version of the problem no matter how high the Reynolds number. Figures 2(c) and (d) of the main paper show schematically the critical points and their branch-cuts for these quasi-modes. It is found that as the eigenvalues are followed along the contours in figure 4(a) across the branch-cuts into figures 4(b), (c), (d) and (e), the critical point nearest the wall can cross the real z-axis, giving a quasi-mode like in figure 2(b) of the main paper, but then go on to cross the imaginary z-axis as well, giving quasi-modes like that shown in figure 2(c) of the main paper. They can even spiral around the origin and emerge again in the first

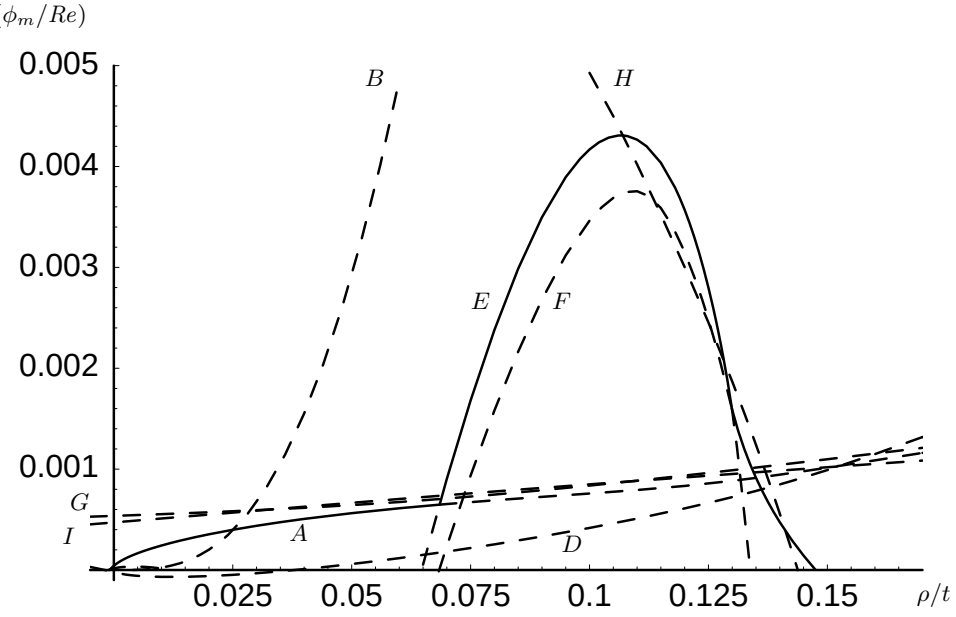

FIGURE 3. Growth rates predicted by saddles of (4.2) when $\beta/\rho = 0.007$ and $\zeta/t = 0$, over a larger ρ/t range than shown in figure 9 of the main paper. Solid lines indicate the dominant saddle, dashed lines indicate saddles that are either subdominant, or irrelevant.

quadrant, like in figure 2(d) of the main paper. This latter mode has a critical point such that Lin's rule, see Lin (1955), which is based on a local analysis, would suggest that the path can be taken along the real z-axis, but our global calculations show that a much more convoluted path is required that does not cross the spiralling branch-cut. In fact, the contours below H in the lower right-hand corner of figure 4(e) have critical points that can cross the real z-axis a second time, giving twice the usual critical point phase jump.

However, it seems that there is no corresponding viscous solution to the cases shown in figures 2(c) and (d) of the main paper, as there was for the conventional quasi-mode shown in figure 2(b) of the main paper. Before the critical point crosses the imaginary z-axis, the origin is engulfed by the viscous wedge lying above the critical point shown in figure 2(b) of the main paper. Once this has happened, the path in the complex z-plane can no longer reach the origin without entering the viscous region, and viscosity then has a leading order effect on the dispersion relation. In such a case, letting the viscosity become arbitrarily small does not allow us to recover the inviscid solution. This is in contrast to the usual effect of viscosity. Although viscosity represents a singular perturbation to the inviscid problem, it only has a leading order effect on the inviscid eigenvalues if the viscous critical-layer is thick enough to overlap the viscous wall layer, see Drazin & Reid (1981) (if the imaginary parts of the eigenvalues are small, then an appropriately large Reynolds number can have a leading order effect on the stability, but this is not the present situation). Since the thickness of these layers can be made arbitrarily small by increasing the Reynolds number, the eigenvalues of the viscous problem for fixed frequency or wavenumber will asymptote to the inviscid eigenvalues once the layers have separated. For example, in Healey (1995) the merging/separating of the viscous layers can be seen at a well-defined Reynolds number, and produces a relatively sharp change in the eigenvalues, leading in that case to a kink in the neutral stability curve. The

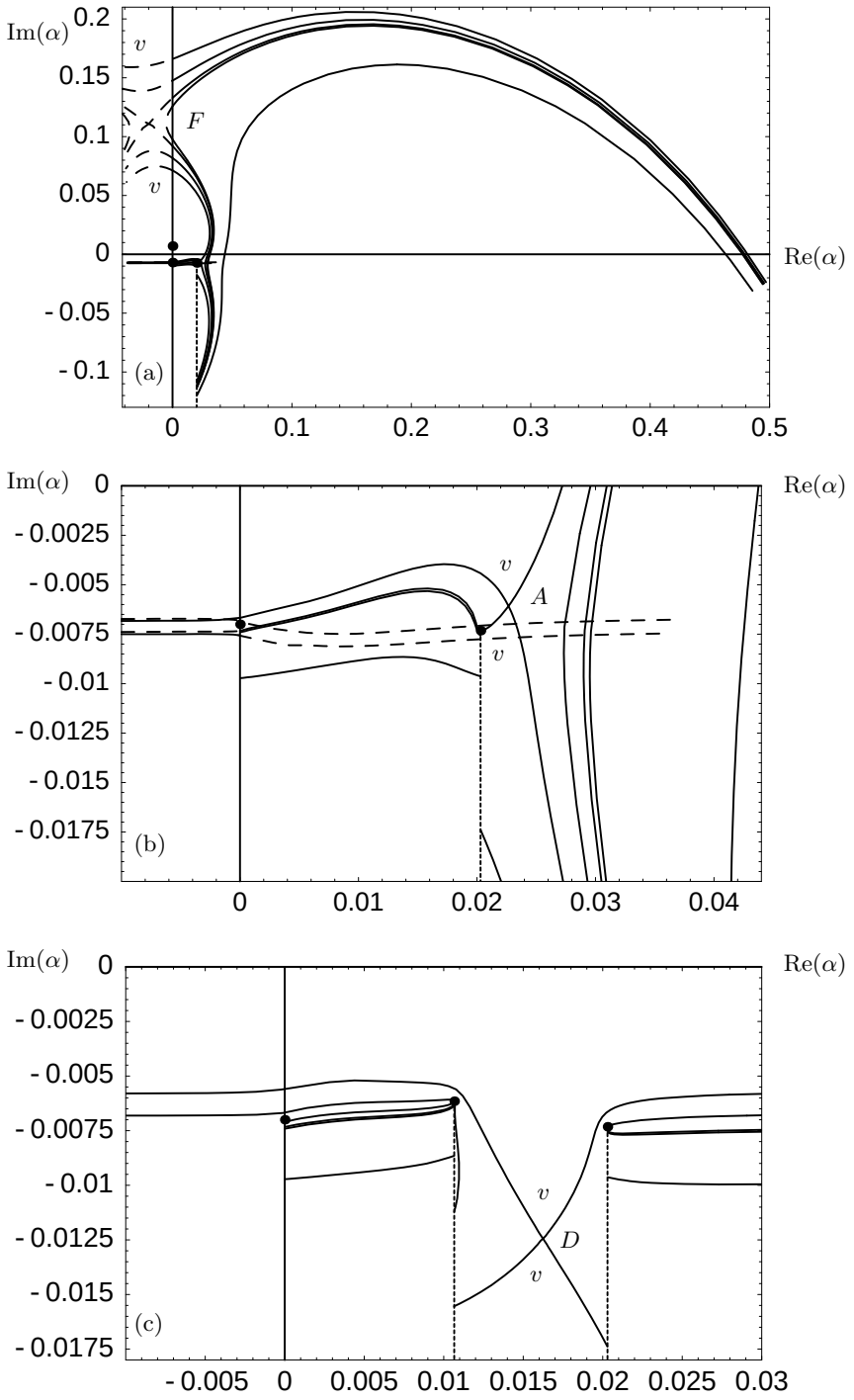

FIGURE 4. Contours of constant $\mathrm{Re}(\phi_m)$ defined by (4.2) when $\beta/\rho = 0.007$, $\rho/t = 0.1342$ and $\zeta/t = 0$. Solid lines indicate convergent eigenfunctions, dashed lines divergent eigenfunctions, disks are branch-points, vertical dashed lines drawn from branch-points are branch-cuts (branch-cuts from branch-points at $\alpha = \pm \mathrm{i}\beta/\rho$ not shown, and their associated Riemann surfaces are superposed). Valleys of saddles are shown by v, hills by h. Contours are at the levels of the saddles A, D, F, G, H and I shown in figure 3 at $\rho/t = 0.1342$. (a) and (b) show one surface, (c) shows a second surface, (d) and (e) show a third surface, (d) also has a small part of a fourth surface near I.

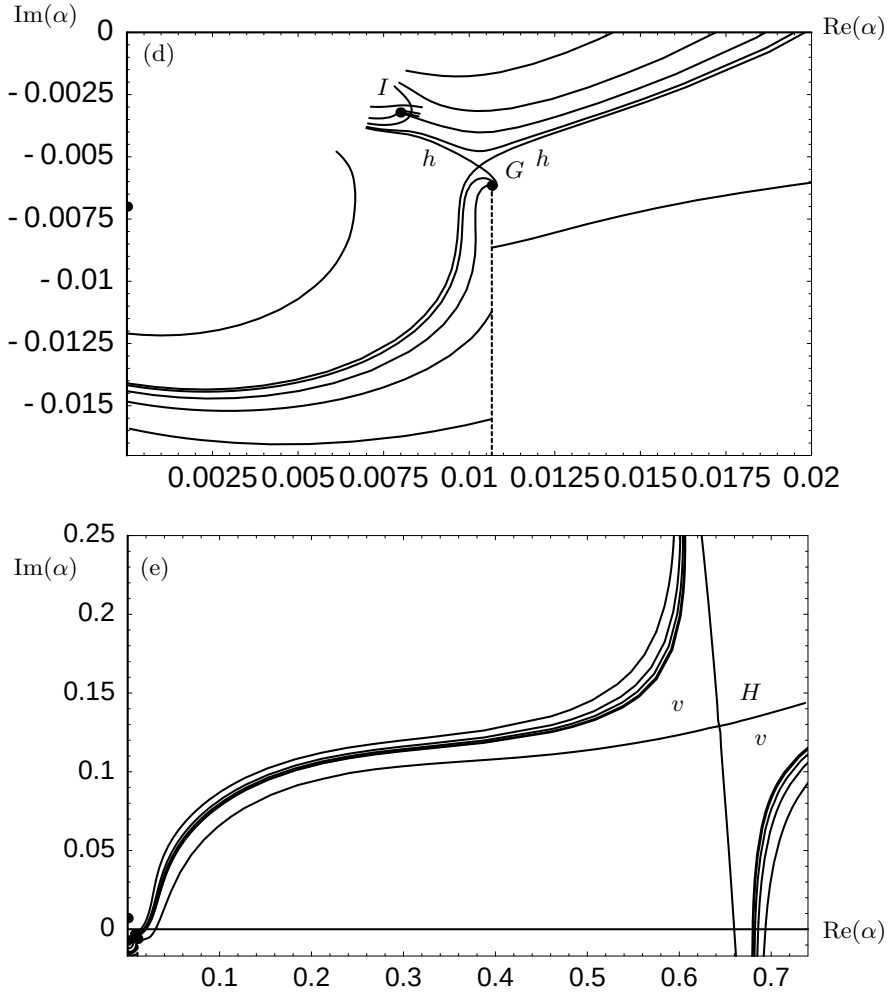

FIGURE 5. Figure 4 continued.

difference in the present case is that while decreasing the viscosity reduces the size of the viscous critical-layer (the viscous bulge surrounding z_c in figure 2(b) of the main paper), it does not affect the size and location of the sector where the viscous solution dominates, which means that for quasi-modes like those in figures 2(c) and (d) of the main paper viscosity always dominates the solution, no matter how small the viscosity is. We shall therefore ignore the quasi-modes G, H and I in what follows since they do not correspond to solutions of the viscous problem.

The contours of constant growth rates have been mapped out in the complex α-plane for several more values of ρ/t (in addition to the value $\rho/t = 0.1342$ used to construct figure 4) so that the dominant saddle can be identified all along the $\zeta/t = 0$ axis. The results are included in figure 3. In summary, the following saddles are unstable and dominant when $\zeta/t = 0$: C for $-0.00113 < \rho/t < -0.00082$; A for $-0.00082 < \rho/t < 0.0685$; E for $0.0685 < \rho/t < 0.1299$; F for $0.1299 < \rho/t < 0.1475$. Saddle E is a quasi-mode for $\rho/t > 0.128$ and F is a quasi-mode for its whole unstable range.

The saddles A – F in figure 3 have been continued to positive ζ/t and any values of ζ/t

where saddles have neutral growth rates identified. The neutral curves for these saddles have been mapped out in the $(\rho/t, \zeta/t)$ plane. Values of ρ/t where the growth rate curves for pairs of saddles intersect in figure 3 have also been identified and followed in the $(\rho/t, \zeta/t)$ plane. A further three saddle coalescence points have been found in addition to the one shown in figure 10 of the main paper. The results are presented in figure 6. Note that the line DE is the same as DF, and AE is the same as AF. The change in labels occurs because these lines pass over the saddle coalescence point of E and F. There are also saddle coalescence points for the pair A and D and for the pair A and E (or equivalently, A and F). The existence of these saddle coalescence points, including the one between A and B, shown most clearly in figure 10 of the main paper, means that the labelling of the neutral curves can become highly ambiguous, with the curve labelled F in figure 6(b) evolving from F to E to A to B as ρ/t is reduced to the values shown in figure 10 of the main paper.

REFERENCES

Drazin, P. G. & Reid, W.H. 1981 *Hydrodynamic Stability Theory.* CUP.

Healey, J. J. 1995 On the neutral curve of the flat-plate boundary layer: comparison between experiment, Orr–Sommerfeld theory and asymptotic theory. *J. Fluid Mech.* **288**, 59–73.

Hinch, E. J. 1991 *Perturbation Methods.* CUP.

Lin, C. C. 1955 *Hydrodynamic Stability Theory.* CUP.

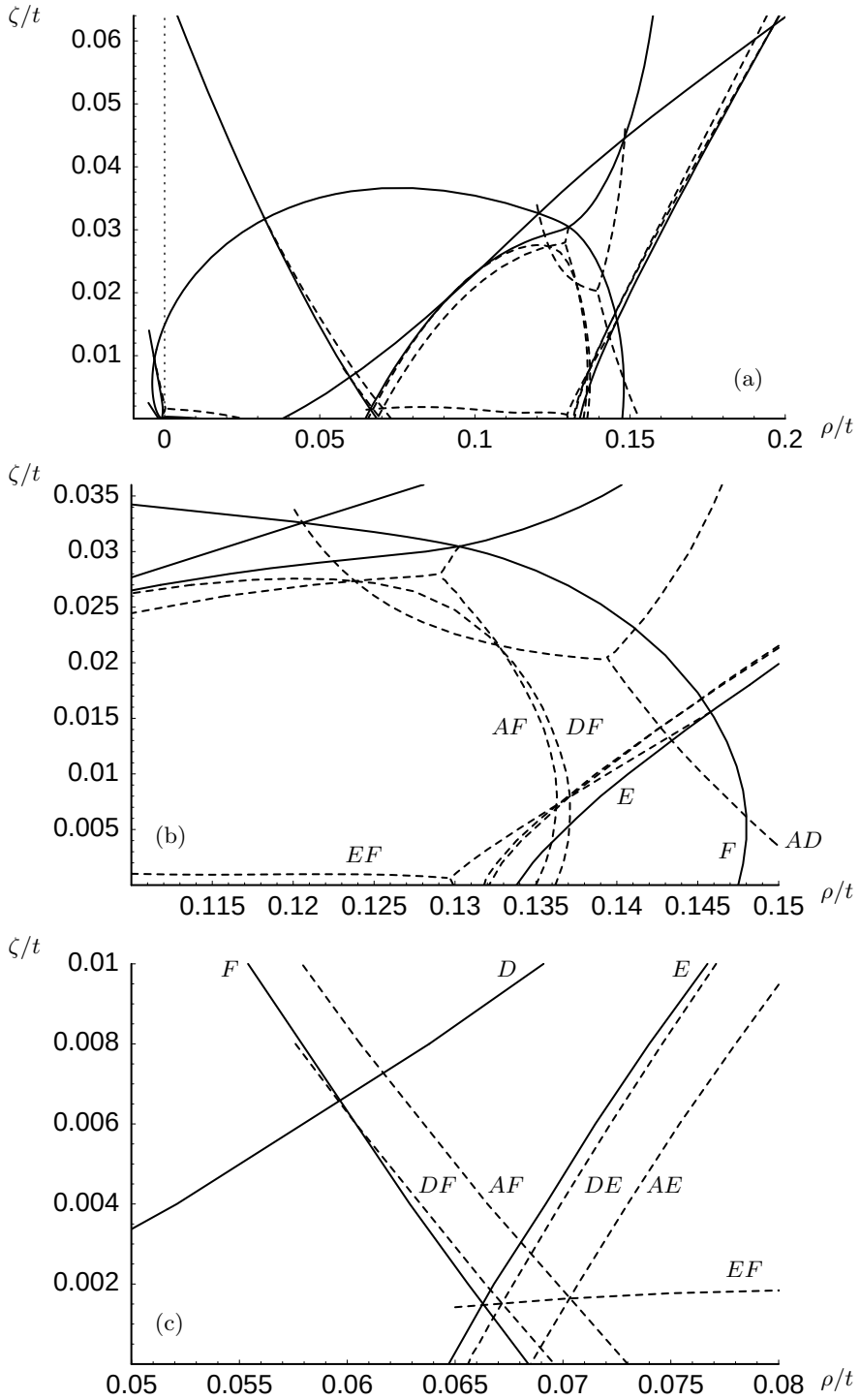

FIGURE 6. Solid lines are neutral curves and dashed lines are where pairs of saddles have equal growth rates for $\beta/\rho = 0.007$. (a) Extension of figure 10 of the main paper, including the saddles E and F. Details of (a) are shown in (b) and (c). As in figure 10 of the main paper, dashed lines are labelled by the pair of saddles that have equal growth rates along them, solid lines by their respective saddles. Labels apply at $\zeta/t = 0$, but they can change when $\zeta/t > 0$ because of saddle coalesence points. The dashed line passing through $\rho/t = 0.1318$, $\zeta/t = 0$ is AE, and through $\rho/t = 0.1321$, $\zeta/t = 0$ is DE.